A Two-Way Fluid-Structure Interaction Approach to Investigate Hemodynamics and Mechanical Behavior of Cerebral Aneurysm: A Computational Study

Haneen Qirba[1], Saud Khashan[1], Tariq Darabseh[1,2,*]

[1]Mechanical Engineering Department, Jordan University of Science and Technology, P.O. Box 3030, Irbid, 22110, Jordan
[2]Aeronautical Engineering Department, Jordan University of Science and Technology, P.O. Box 3030, Irbid, 22110, Jordan

Abstract

In this study, we computationally examine the biomechanics of a cerebral aneurysm (CA) using a two-way Fluid-Structure Interaction (FSI) approach. The integrated approach using computational fluid dynamics (CFD) and computational solid dynamics (CSD) aims to connect the intra-aneurysmal environment and the rupture process and assess the risk of aneurysm rupture. The velocity distribution and the wall shear stress (WSS) were calculated within these aneurysms. The dynamic response of cerebral aneurysms was predicted using CSD. We conducted parametric analyses based on CA aspect ratio (AR) and viscosity sensitivity analysis to allow easier exploration of their effects. The findings demonstrate that velocity values decrease as aneurysm size increases, associated with the drop in WSS. Results demonstrated how the wall deformation associated with the growth of CA aspect ratios causes strain and raises the danger of aneurysm rupture.

1. Introduction

FSI involves the interaction between a structure and a flowing fluid, encompassing the interplay of fluid and solid motions and their relationships. FSI problems consider the impact of fluid velocity and pressure, which are influenced by structural deformations. In recent times, there has been a growing emphasis on engineering projects incorporating lighter and more flexible structural designs. These fluid-conducting structures pose complex multi-physical challenges that are often difficult to handle. Numerical simulations have emerged as crucial tools in various engineering fields, but their effectiveness is hindered by the need to predict flow regions that are inaccessible through experiments. Achieving an accurate numerical simulation of FSI problems is challenging due to the strong coupling between fluid and structure. Implementing the FSI model successfully within the CFD framework and transient structure solvers can provide a reliable tool for solving flow deformations and updating meshes. Convergence of the coupling algorithm that links the fluid and structure domains is essential [1]. The two-way FSI approach is suitable for problems where both the solid and fluid flow mutually influence each other [2]. Hemodynamics simulations using CFD rely on various factors such as the behavior of blood (Newtonian or non-Newtonian), the conditions of inflow and outflow, the

availability of accurate in-vivo measurements, and the ability to model vascular wall motion [3]. Considering these factors, CFD has the capability to analyze the hemodynamic environment of blood flow in cerebral aneurysms and predict abnormal shear stress. These abnormalities in shear stress can serve as indicators of weaknesses in the vessel wall [3]. Successful simulations using CFD for cerebral aneurysms can provide significant insights into flow conditions both within arteries and within the aneurysm itself. This information can assist in establishing a link between flow patterns and aneurysm initiation, development, and rupture risk. CFD is becoming a more accurate method for determining WSS in human aneurysms [1].

There are many articles addressing FSI issues related to cerebral aneurysms in the literature. Previous studies have diligently emphasized the crucial role of CFD in the detection and treatment of CA. The majority of these studies have confirmed the significance of WSS during the initiation because of its impact on the endothelial layer. Poueinak et al. [4] emphasize the importance of blood flow in the occurrence of CA hemorrhage. Their study examines the blood flow dynamics in the Internal Carotid Intracranial (ICA) growth, focusing on the effects of coiling. Their CFD analysis shows that reduced coiling porosity significantly lowers WSS and oscillatory shear index (OSI), particularly in situations with high blood viscosity. Sabernaeemi et al. [5] reported that stent-

assisted coiling effectively treats intracranial aneurysms but emphasizes the risk of vasculature deformation. One-way FSI is used to study four intracranial aneurysms (ICA). Stents significantly reduce hemodynamic parameters, except OSI and aneurysm neck inflow. Intervention effects vary, focusing on the overlooked hemodynamic effect of aneurysm deformation. In cases of significant aneurysm deformation, stents alone can improve hemodynamic factors, according to the study. Salavatidezfouli et al. [6] examined stent deformations in ICA aneurysm treatment using CFD. Four aneurysms with different characteristics were studied for blood circulation and flow patterns. The results showed that the aneurysm deformation decreased blood flow into the sac, lowering sac wall velocity and oscillatory shear index. Stent-induced deformation was most noticeable in high OSI aneurysm walls. Shen et al. [7] performed a computational investigation to assess the influence of blood flow on the formation of aneurysms in the ICA. Their primary aim was to clarify the main factors contributing to an aneurysm rupture by evaluating pressure distribution and WSS. Their CFD analysis revealed a direct correlation between the growth of an aneurysm and its orientation and location. The study revealed that the aneurysm's average WSS was considerably lower than the exterior.

He et al. [8] used FSI techniques to study how arterial wall compliance and microcirculation affect arterial hemodynamics and blood flow. Savabi et al. [9] performed numerical FSI analyses on 3D models of the aortic arch, specifically looking at various fluid-related hemodynamic parameters such as velocity, WSS, pressure distributions, as well as stress and deformation in the solid domain. Cho et al. [10] utilized FSI to make predictions regarding the likelihood of CA rupture. Sun et al. [11] conducted an FSI study focusing on the impact of aneurysm AR, artery thickness, and hypertension. Saqr [12] compared the Navier-Stokes simplification with the non-Newtonian power-law model by investigating a ruptured middle cerebral artery, aiming to identify differences between the two approaches. Gholampour and Mehrjoo [13] employed CFD models to investigate changes in hemodynamics and the potential risk of rupture in bifurcation middle cerebral aneurysms. Isaksen et al. [14] conducted FSI simulations with patient-specific geometries to examine the effects of wall stress and displacement in cerebral aneurysms.

Jiang et al. [15] investigated the influence of morphology, particularly the shape, of a saccular aneurysm on the probability of rupture. By employing computer models to simulate different scenarios, researchers found that increased blood viscosity significantly increased the chances of rupture, while specific coiling techniques reduced this risk. Altering the coil's properties affected factors such as pressure and flow inside the enlarged vessel, providing valuable data for potential preventive measures. Sadeh et al. [16] used CFD simulations to investigate the impacts of blood hematocrit and coiling on the aneurysm risk of aneurysm rupture based on an angiography image. They comprehensively evaluated WSS, aneurysm wall pressure, and oscillatory shear index at different blood viscosities. One-way FSI is applied to simulate the non-Newtonian, pulsatile blood flow through the aneurysm sac. The pulsatile bloodstream was designed

by Hariri et al. [17] using CFD simulation by solving Reynolds Average Navier-stocks equations. They investigated the pressure, oscillatory shear index, and WSS on the sac wall of CA during the blood cycle. They found that the maximum value of WSS was near the neck of the sac, while the oscillatory shear index was near the aneurysm dome.

In their study, Kleinstreuer et al. [18] conducted simulations to evaluate the impact of a physical hemodynamic model coupled with wall mechanics on the treatment of Abdominal Aorta Aneurysm (AAA). Xenos et al. [19] utilized simulations with reconstructed models from Computerized Tomography (CT) scans of AAA patients to predict potential rupture locations. Scotti et al. [20] developed multiple models considering transient flow conditions to investigate the effects of wall thickness on the peak value of WSS.

Rostam-Alilou et al. [21] performed a comprehensive analysis of FSI to explore the intricate interactions between blood flow and vessel tissue. The study conducted FSI analysis to simulate the interactions between blood and vessels, shedding light on the importance of pre-existing arterial occlusions in altering hemodynamic behavior. Variations in blood pressure and velocity were found to increase the risk of remodeling artery tissue and developing aneurysms. The researchers specifically focused on dynamic simulations of blood flow to investigate the behavior of CA hemodynamics. They observed that assuming Newtonian viscosity resulted in more stable blood flow, whereas non-Newtonian assumptions led to instability. Furthermore, they noted that the size of the aneurysm and the angle of bifurcation significantly influenced the inflow of aneurysms, which is critical for treatment.

Shine et al. [22] used computational methods to analyze the hemodynamics of arteries in the circle of Willis with the aim of identifying potential sites for CA development. Their analysis indicated that junction locations within the circle of Willis displayed high values of WSS, posing a greater risk for aneurysm initiation based on the WSS distribution. They also observed that decreased wall elasticity led to reduced WSS values. The arteries showed localized Von Mises stress, which could contribute to an increased susceptibility to aneurysm formation and rupture. In a separate study, Abdollahi et al. [23] employed CFD and two-way FSI interaction methods to investigate aneurysm rupture and assess the impact of various hemodynamic parameters.

Almomani et al. [24] investigated that the carotid artery geometry is a main cause of blood flow-related carotid artery diseases. They focused on the changes that happened to the internal off-plane angle of the carotid artery. They investigated the hemodynamic parameters that lead to the formation of plaques and atherosclerosis. They performed steady, three-dimensional CFD computations with 0.3 mm/sec inlet velocity, no-slip boundary conditions, and rigid walls.

In their study, Paz et al. [25] concentrated on examining the impact of coil embolization in a realistic CA, with a specific emphasis on the thickness of the vessel wall and aneurysm. They conducted transient FSI simulations, analyzing multiple models and comparing the equivalent stress levels before and after coil embolization.

In a different study, Khe et al. [26] utilized a large saccular aneurysm located at the bifurcation of the basilar artery to replicate blood flow in cerebral arteries. They examined the hydrodynamic and mechanical characteristics using different modeling approaches, including the rigid-wall assumption, one-way FSI, and two-way hydro-elastic model. According to Fattahi et al. [27], the size of a saccular aneurysm and its connecting vessel diameter affect blood flow characteristics. They examined coiling-treated aneurysm WSS, pressure, and OSI. The study found that increasing the connecting vessel's diameter directly reduced OSI on the bulging vessel's surface using computational modeling of non-Newtonian blood flow in different aneurysms. As the connecting vessel diameter increased, the mean WSS decreased. Fattahi et al. [28] examined how blood vessel size affects cerebral aneurysm rupture risk. The study detailed ICA aneurysm blood flow dynamics with different parent vessel sizes. CFD was used to model blood flow and compare WSS, OSI, and pressure distribution. The parent vessel's size affected the minimum WSS.

Hajirayat et al. [29], through FSI simulations, investigated blood hemodynamics and the risk of rupture in cerebral aneurysms with various neck geometries. They observed that blood hemodynamic parameters increased after the formation of an aneurysm, with the WSS increasing by a factor of 4.1-6.5 compared to a healthy patient. Furthermore, they found that a CA with a circular neck had a 40.8% higher likelihood of artery rupture compared to an aneurysm with an elliptical neck. Sheidani et al. [30] examined blood hemodynamics in cerebral aneurysm development, specifically within the Internal Carotid Artery. Using computational fluid dynamics, they considered transitional, non-Newtonian, and incompressible conditions to identify high-risk regions on the aneurysm wall. Comparative analysis of OSI and WSS at different blood flow stages revealed insights into the impact of blood viscosity and coiling treatment. Adjusting coiling porosity influenced maximum OSI, with variations observed based on patient characteristics.

Tan et al. [31] utilized FSI simulations to predict WSS and hemodynamic factors associated with the growth and rupture of thoracic aortic aneurysms. Lantz et al. [32] and Alimohammadi et al. [33] investigated WSS changes influenced by wall motion in the human aorta using FSI simulations. Torii et al. [34] and Bai-Nan et al. [35] employed FSI to conduct hemodynamic analyses of coronary arteries through CFD simulations, focusing on WSS. Luo et al. [36] analyzed FSI models involving rigid walls, vessel deformation, WSS, and flow distribution in arterial bifurcations to obtain accurate flow patterns. Jahangiri et al. [37] and Frecentese et al. [38] performed dynamic modeling of stenosed arteries using FSI simulations with different non-Newtonian blood viscosity models. Torii et al. [39] identified hypertension as a high-risk factor for aneurysm rupture based on blood pressure measurements. Ahmed et al. [40] investigated the effects of hypertension and elasticity models on aneurysm rupture through computational coupled FSI analysis. Feng et al. [41] simulated the growth and rupture of cerebral aneurysms using numerical aneurysm models, considering both straight and curved geometries, in FSI simulations. Torii et al. [42] analyzed a wall structure model of patient-specific cerebral aneurysms using FSI simulations. Torii et al. [43] and Valencia et al. [44] studied the influence of wall thickness in FSI simulations. Takizawa et al. [45] analyzed patient-specific cerebral aneurysms through FSI simulations. Bazilevs et al. [46, 47] compared WSS and wall tension using FSI simulations to investigate hemodynamic factors. Takizawa et al. [48] examined various CA models based on size and location using FSI simulations with patient-specific models. Lee et al. [49] simulated FSI using patient-specific models to explore differences between ruptured and unruptured aneurysms. Qiu et al. [50] investigated the relationship between morphological properties and WSS using simplified FSI models, considering parameters such as the maximum angle of bifurcation and constant wall thickness, to assess the effect of morphological properties on WSS. Shamloo et al. [51] studied the impact of wall thickening in cerebral aneurysms and the effects of endovascular coiling treatment using FSI simulations. Valencia and Torres [52] studied the blood pressure and hypertension effects on aneurysm rupture using FSI simulations. Avolio et al. [53] studied the effect of hypertension, pulsatile blood flow, and oscillatory blood pressure on aneurysm rupture.

Shawish et al. [54] used CFD simulation in other applications as air-to-air energy recovery ventilators examined numerically using a 3D CFD simulation. The well-known Navier-Stokes, Energy, and continuity nonlinear differential equations describe the incompressible steady-state airflow. Saraireh [55] presented a three-dimensional CFD simulation of fluid flow and heat transfer for two types of heat sinks. CFD simulations are used to solve the fluid flow and energy equations and temperature as boundary conditions. Alshare et al. [56] developed gas flow and heat transfer through a wavy microchannel. Rashid and Singh [57] studied the effects of inertia and buoyancy forces numerically investigated using fluid dynamics and heat transfer characteristics in CFD simulations for micro-heated cylinders in an unconfined flow regime.

From the author's point of view, the mechanical behavior of cerebral aneurysms using two-way FSI as a computational study needed to be covered more in the literature. This problem was solved, simulated, and compared with the published results. The study aims to demonstrate the importance of FSI as a computational tool. Also, FSI establishes a better understanding of the human arteries biomechanics, particularly for CA cases in terms of initiation, development, and rupture. In addition, to develop a two-way FSI model that predicts the dynamic responses of cerebral aneurysms. In addition, the CFD is utilized to assess the aneurysmal WSS and velocity distribution for cerebral aneurysms at different aspect ratios. Finally, we simulate the CA in various sizes on WSS and the risk of rupture.

2. Problem Formulation

The problem formulation of this paper is outlined in the following sections.

2.1. FSI System Coupling

System coupling makes the independent physics solvers of any system and the external data sources of that system work together in a coupled Multiphysics analysis. System coupling is performed by setting up the physics behind the systems, defining data transfer variables and regions, also specifying the analysis settings. There are two types of coupling methods, steady and transient. The steady-state approach is utilized when all the participants exhibit steady-state or static behavior. On the other hand, the transient system is employed when all participants exhibit transient behavior [11]. In our study, the mechanical and fluid flow systems are considered transient systems.

Once the systems are connected through the system coupling component, the solution updates are automatically initiated whenever the system coupling solution cell is updated. For our study, we implemented FSI using two commercial software programs available within the ANSYS package: Transient Structural for CSD and FLUENT for CFD. The setup of the system coupling simulations involves determining the analysis settings such as the time step size, end time, and the number of coupling iterations.

Next, we manage the data transfer and simulation sequences between the two numerical solvers. Before running the coupled system for cerebral aneurysms, we configure the physics for each participant and define the data transfer variables and coupling regions accordingly. Additionally, we establish the necessary coupling-related settings. The simulation setup encompasses crucial steps such as assigning material properties, defining boundary conditions, and selecting appropriate numerical techniques for the models employed in the analysis.

2.2. Geometry

In recent years, the development of patient-specific blood flow modeling has progressed significantly, driven by advancements in imaging, modeling, mesh generation, computation, and visualization technologies. The simulations aim to explore hemodynamic factors that impact the initiation and progression of cardiovascular diseases, predict surgical intervention outcomes, or assess the effects of electromechanical assist devices. In our study, we employed two geometric models to approximate the shape of aneurysms. The first model represents a non-bifurcating artery with a spherical aneurysm dome, as depicted in Figure 1a. The second model represents a T-shaped bifurcating artery with a spherical aneurysm dome, as shown in Figure 1b. The models consist of two distinct regions: the aneurysm dome and the arteries. These models were derived from actual patient MRI angiography images existing in the literature, specifically from Bazilevs et al. [46, 47].
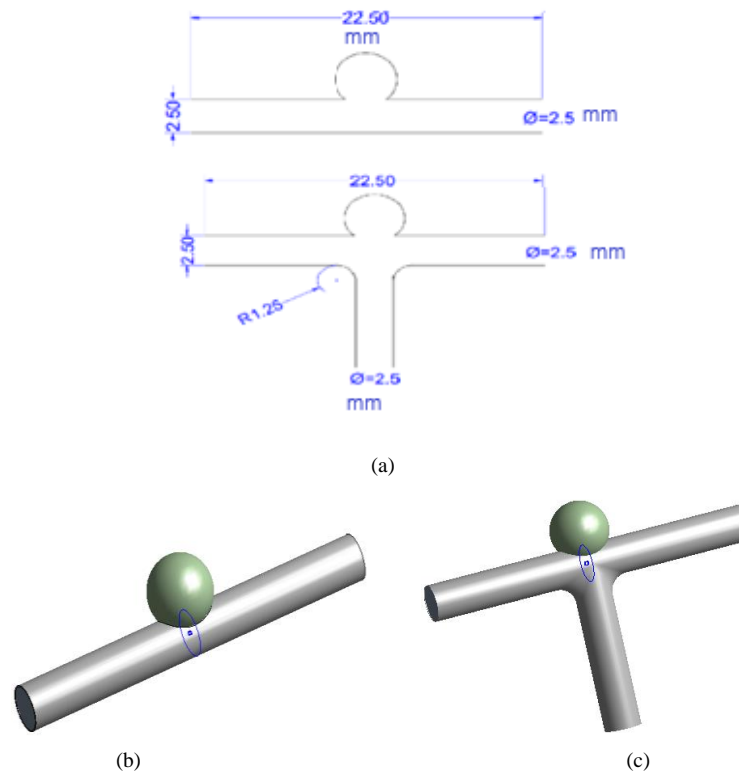
Figure 1. (a) models' schematic diagram (all dimensions in mm), (b) non-bifurcation model, and (c) T-shaped bifurcation mode.

The primary artery, which serves as the standard for both models, is considered to be a fixed-diameter tube with a diameter (d_t) of 2.5 mm and a length (L) of 22.5 mm. In the case of the second model, representing the bifurcation artery, the branch artery has the same diameter as the main artery but with a length (L) of 10 mm. The neck region, where the aneurysm connects to the artery, is approximated as an elliptical shape with an apoapsis radius of 1.25 mm. To ensure a smooth transition in geometry between the arteries, a 1.25 mm fillet is introduced. The approximate spherical aneurysm has a diameter (d_a). The sizes considered for unruptured cerebral aneurysms range from 0 mm to 14 mm, with a 2 mm increment, based on the study by Ishibashi et al. [58]. The AR is defined as the ratio of the aneurysm diameter (d_a) to the artery diameter (d_t).

$$AR = \frac{d_a}{d_t} \tag{1}$$

The thickness of both the main artery and branch artery walls is assumed to be uniform and equal to 0.46 mm, as stated in the study by Sherif et al. [59]. The aneurysm thickness varies between 0.03 mm and 0.4 mm, according to research by Isaksen et al. [14]. Based on clinical data for unruptured aneurysms, Steiger et al. [60] estimated the wall thickness of an aneurysm to be approximately 1.2% of the aneurysm diameter. The following equation is used to determine the aneurysm wall thickness, allowing for the estimation of the relationship between the AR and other variables:

$$t_{an} = 0.012da \tag{2}$$

2.3. Computational Mesh

The grid generation for this problem is accomplished using ANSYS meshing. The element sizing for the idealized geometry without bifurcation is set at 0.1 mm for both the solid and fluid domains. The total number of elements is 1.9×10^6. The element sizing for the solid domain in idealized bifurcation geometry is 0.1 mm, while for the fluid domain, it is 0.3 mm. The total number of elements is 2.5×10^6.

The second mesh controller is inflation, which allows for the addition of layers along specific wall artery edges to enhance the dependence of the results. The inflation zone encompasses ten layers, each with a thickness of 1.2, resulting in a total thickness. This growth rate covers 10% of the diameter of the primary artery. In the independence test, the maximum within-cluster sum of squares (max-WSS) was used as the value to be tested. The max-WSS remained constant regardless of changes in the element size. The chosen value for the element size was determined when the mesh results differed by less than 2% from the previous mesh results. Figure 2 displays a sample of the mesh employed, along with the inflation layers. Additionally, it offers an analysis of mesh independence.

(a)   (b)

(c)
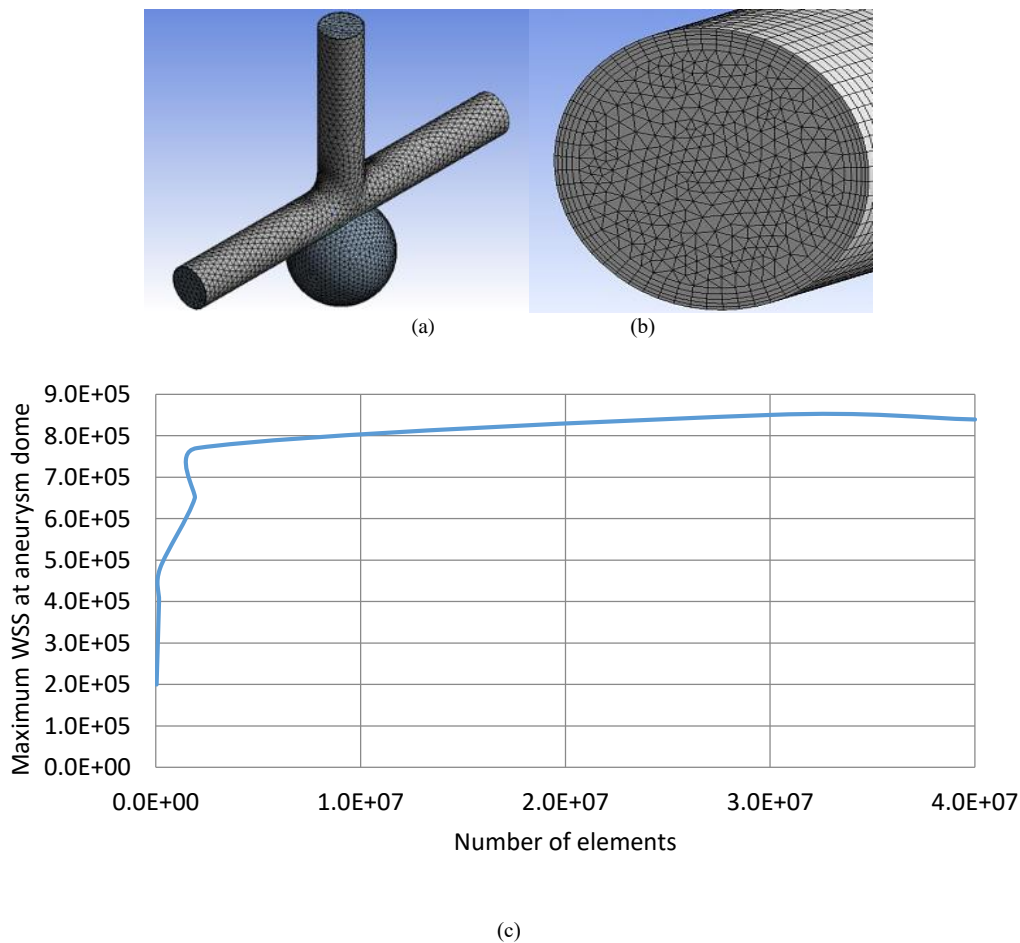
Figure 2. (a) the meshing of the interior (fluid) domain and the outer (solid) domain, (b) zoon on the mesh of the inlet surface of blood and boundary inflation layers, and (c) mesh independency analysis.

2.4. Material Setup

Blood is a complex mixture consisting of solid components suspended in liquid plasma, making it a multi-phase mixture. The viscosity of blood is influenced by various factors, including its composition, distribution of blood cells, and mechanical properties. Additionally, the blood viscosity is affected by external forces applied and the prevailing physical conditions.

In many cases, the Newtonian blood model is appropriate, particularly in large vessels where shear rates are moderate to high. However, at lower shear rates below $100\ s^{-1}$, non-Newtonian effects become more significant. At shear rates above this threshold, blood can be approximated as a Newtonian liquid [61]. Among the commonly used non-Newtonian blood models, the Carreau-Yasuda and Casson models are popular choices.

In the Carreau-Yasuda model, the viscosity is described by a specific formulation:

$$\mu = \mu_\infty + \frac{\mu_o - \mu_\infty}{(1+(\lambda\dot{\gamma})^a)^{\frac{1-n}{n}}} \tag{3}$$

Here, μ is the effective viscosity and $\mu_\infty, \mu_o, \lambda, \gamma$ and n are material properties described and specified as:

- μ_∞ (Infinite shear viscosity) = 0.0035 kg/m.s.
- μ_o (Zero shear index) = 0.056 kg/m. s
- λ (Time index) = 3.313 s
- n (Power-law index) = 0.3568

In the case of an aged patient, the modulus of elasticity (E) for the arteries is considered to be 0.9 MPa, while for the aneurysm dome, it is taken as 1.4 MPa [60]. Both the arteries and aneurysm dome have a density (ρ) of $1120\ kg/m^3$, and the Poisson's ratio (υ) for the aneurysm dome is 0.4. It is worth noting that the stiffness, yielding, and elasticity of the aneurysm dome in elderly patients are typically lower compared to those observed in younger and healthier individuals [62].

Table 1. Material properties [60]

	Yield strain	Yield stress (MPa)	Elastic modulus (MPa)
Aneurysm dome	0.37 ±0.15	0.5±0.26	1.7±0.8
Aneurysm neck	0.57±0.39	1.21±0.49	3.1±0.9
Arteries	0.37±0.10	1.06±0.13	2.5±1.1

2.5. Governing Equation

In blood flow modeling, the equations described the laminar and incompressible blood flow in arteries given as the conservation of mass and momentum (Navier-Stokes's equations). Here we list them as:

In the modeling of blood flow, the equations that describe the laminar and incompressible blood flow in arteries are based on the principles of conservation of mass and momentum, commonly known as the Navier-Stokes equations. These equations can be written as follows:

$$\frac{\partial\rho}{\partial t} + \nabla.(\rho\vec{u}) = 0 \tag{4}$$

$$\frac{d}{dt}(\rho\vec{u} + \nabla.(\rho\vec{u}\vec{u}) = -\nabla p + \nabla.\vec{\tau} + \rho\vec{g} + \vec{f} \tag{5}$$

Where:
ρ: fluid density
$\vec{u}$: fluid velocity components
$\vec{\tau}$: stress tensor
p: static pressure
$\vec{g}$: gravitational acceleration

$\vec{f}$: body force

In the modeling of the solid artery wall, it is typically assumed to be linearly elastic and isotropic. This allows us to describe the behavior of the solid wall using a constitutive equation, which can be written as:

$$\sigma = E\epsilon \tag{6}$$

$$\nabla.\tau_s + f_s^B = \rho_s\ddot{d_s} \tag{7}$$

Where σ is the stress tensor, E is the tensor of elastic constants, ϵ is the strain tensor, ρ_s is the solid density, τ_s is the solid stress tensor, f_s^B is the body force per unit volume, and $\ddot{d_s}$ is the solid local acceleration.

In the FSI interface, the governing equations for the FSI are described as follows:

$$n.\sigma_s = n.\sigma_f \tag{8}$$

$$\delta_s = \delta_f \tag{9}$$

Where δ is the displacement vector, the subscript s is for the solid and the subscript f is for the fluid. The fluid (blood) and solid deformation are solved by the integrated Finite Element Analysis (FEA) and Finite Volume Analysis (FVA) in ANSYS 19.1.

2.6. Boundary Conditions

The periodic inlet velocity is taken to have an ultimate velocity of 0.5 m/s and a minimum velocity of 0.1 m/s, and the duration of each period is 0.5 seconds (Figure 3). This inlet velocity is used in a CA simulation [63]. It is implemented in ANSYS as a user-defined function (UDF). On the arterial wall, the no-slip condition is applied. The pressure outlet value is set to 100 mmHg [64, 65]. It is worth mentioning that other works [4, 6] accounted for the pulsatile nature of blood flow inside the vessels using prescribed mass flow rate at the inlet and pressure value at the outlet.
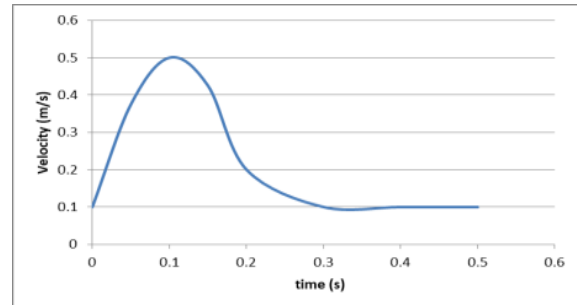
Figure 3. Pulsatile velocity versus time

3. Results and Discussion

The simulation yielded several key results, which are now discussed and explained in detail:

3.1. Viscosity Modeling Analysis

In this study, we examine the impact of viscosity models, specifically the Newtonian and Carreau viscosity models. The Carreau model is commonly employed to capture the non-Newtonian behavior of blood. Our comparative analysis focuses on bifurcation and non-bifurcation geometries, investigating pressure predictions, velocity, and WSS.

Both viscosity models yield identical pressure patterns, as depicted in Figure 4. The color scheme assigns red to

the highest values and blue to the lowest values. Figure 4 illustrates an instance of pressure contours, wherein the contours are influenced by the morphological parameters of each aneurysm and the flow conditions at the inlet and outlet. The pressure drop between the inlet and outlet measures 100 Pa. Since blood is incompressible, the flow rate is solely determined by the pressure difference (Δp) between the inlet and outlet. Consequently, regardless of whether the system pressure is low or high, the flow remains the same as long as the pressure differential between the inlet and outlet remains constant.

Similar to the pressure field, both viscosity models predict comparable velocity fields. Velocity vectors are presented for both geometries at incremental growth rates, corresponding to various aspect ratios of the aneurysm. Additionally, we provide the predicted streamlines. Notably, the velocity in the dome region is slower compared to the arteries, as illustrated in Figure 4. The dome region exhibits near-zero velocities. Across all cases, the streamlines and vectors demonstrate negligible dependence on the selected viscosity model.

According to the findings of this study, regions with low velocities exhibit a prevalence of low WSS. However, the sensitivity of WSS predictions to the choice of viscosity model is more pronounced in these low-velocity regions. This sensitivity diminishes in regions with high velocities. In particular, the sensitivity of WSS to the viscosity model is minimal in the arteries but noticeable in the dome region of the aneurysm.

The discrepancies between the viscosity models become evident in the dome area of the aneurysm. When the AR exceeds 4, both viscosity models yield identical WSS predictions. However, for lower AR values, the difference amounts to approximately 10% for the non-bifurcation geometry and 7% for the bifurcation geometry.

In the following section, a more representative comparison is conducted using the area-averaged Wall Shear Stress($\overline{WSS}$) and strain as predicted under the two-way FSI coupling.

Figure 5 shows the relation between the predicted $\overline{WSS}$ ($= \frac{1}{A} \int WSS.dA$) and the aneurysm growth sizes for both viscosity models. It is observed that $\overline{WSS}$ decreases with increasing the AR. This means as the aneurysm size grows, that the velocity decreases inside the dome, causing a lower in $\overline{WSS}$. Aneurysm growth becomes a way to deal with changes in WSS that could occur because of medical factors like blood velocity and others. The non-Newtonian predicts higher $\overline{WSS}$ at aspect ratios less than 3.2. This difference in prediction becomes tangible when AR is equal to 0.8. For the AR less than 3.2, the non-Newtonian predicts a higher $\overline{WSS}$; this difference is more tangible for AR equal to 2.4. The smaller aspect ratios present the early stages of aneurysm growth.

3.2. Size Parametric Analysis

In this study, we employ the results obtained from Fluent for the flow field as loading inputs for the solid mechanics problem. Conversely, we utilize the results obtained from the transient structure analysis for the solid mechanics as boundary conditions for the flow field. The investigation focuses on the impact of aneurysm sizes, specifically the change in aneurysm AR.

We analyze the effects of the aneurysm AR on various factors, including artery (wall) deformation, wall stress, Von-Mises stress ($\sigma_{v.m}$), and strain. It is anticipated that WSS plays a significant role in the formation and growth of aneurysms. Particularly, examining the relationship between the distribution of WSS and the AR can contribute to a better understanding of the process of aneurysm growth.

(a)

(b)

(c)
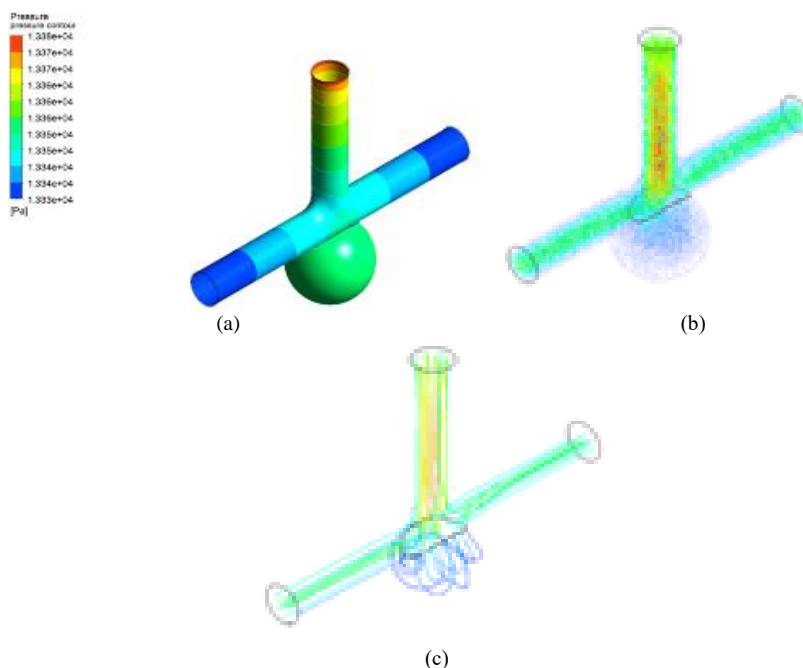
Figure 4. (a) pressure contours, (b) velocity vectors, and (c) velocity streamlines

(a)

(b)
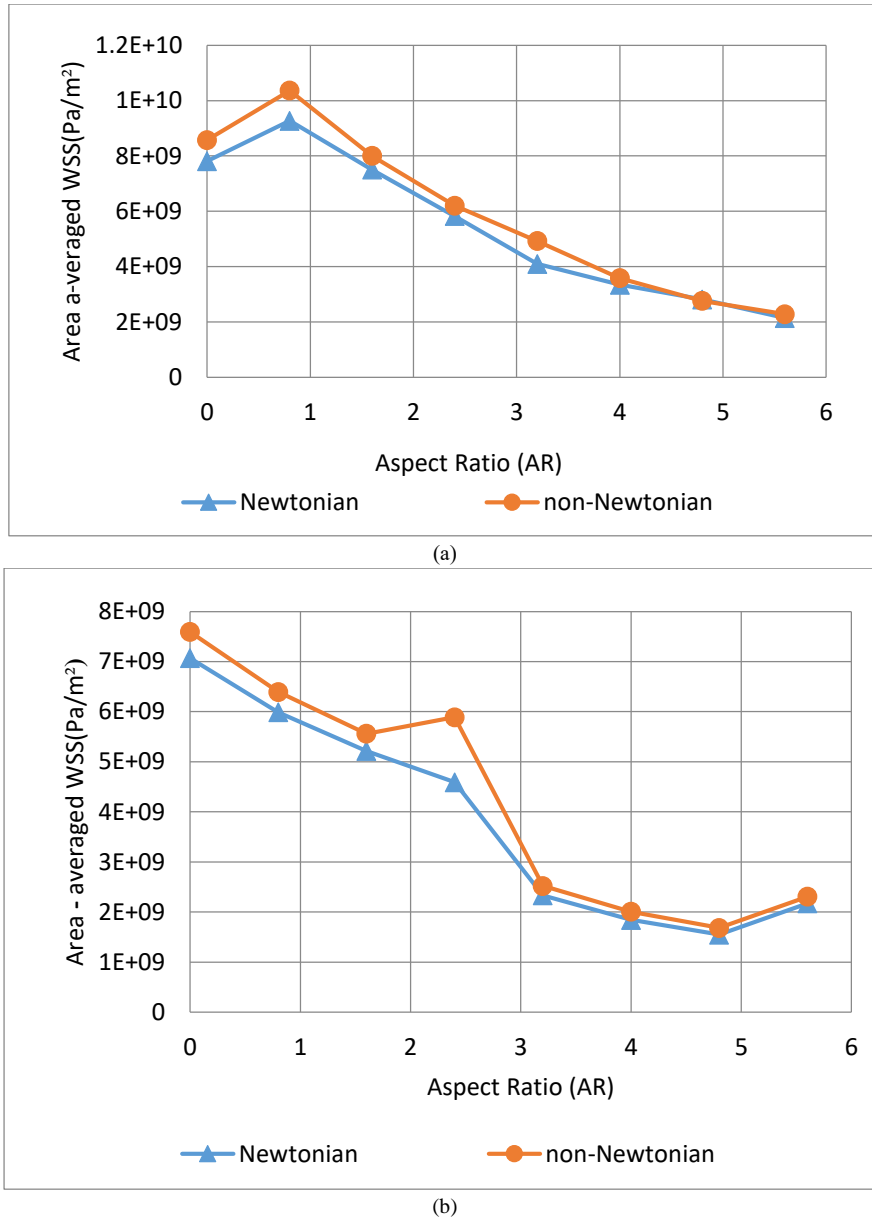
Figure 5. Predicted $\overline{WSS}$ using Newtonian and non-Newtonian viscosity models (a) for non-bifurcation geometry and (b) for the bifurcation geometry.

The growth of an aneurysm leads to a reduction in velocity within the bulging region, resulting in decreased WSS there. Moreover, as the aneurysm continues to grow, the average WSS over the entire area decreases. Figure 4 displays the velocity vector, indicating that the blood directly impacts the bifurcation point. This impingement of flow causes the maximum WSS to occur near the stagnant region of the wall. Prolonged flow impingement can potentially trigger the initiation of an aneurysm as mentioned also by Valencia et al. [66].

The primary criterion for assessing the likelihood of aneurysm rupture is the Von-Mises stress. Materials start deforming when their Von-Mises stress surpasses the yield point. If the value of $\sigma_{v.m}$ within the aneurysm exceeds the yield strength (σ_y), the aneurysm will begin to grow and eventually rupture, as follows:

$$\sigma_{v.m} = \sqrt[2]{\frac{(\sigma_1 - \sigma_2)^2 + (\sigma_2 - \sigma_3)^2 + (\sigma_3 - \sigma_1)^2}{2}} \geq \sigma_y \qquad (10)$$

In a previous investigation conducted by Steiger et al. [60], the yield strength values were found to be approximately 0.5 ± 0.25 MPa for the aneurysm dome and 1.06 ± 0.13 MPa for the arteries. In our current study, we consider these values as a benchmark for assessing the likelihood of aneurysm rupture. Figure 6 illustrates the contours of $\sigma_{v.m}$, with the highest $\sigma_{v.m}$ occurring within the aneurysm region. This elevated stress can be attributed to the thinning of the aneurysm wall compared to the arterial wall. The color red indicates the highest stress value, while blue represents the lowest.
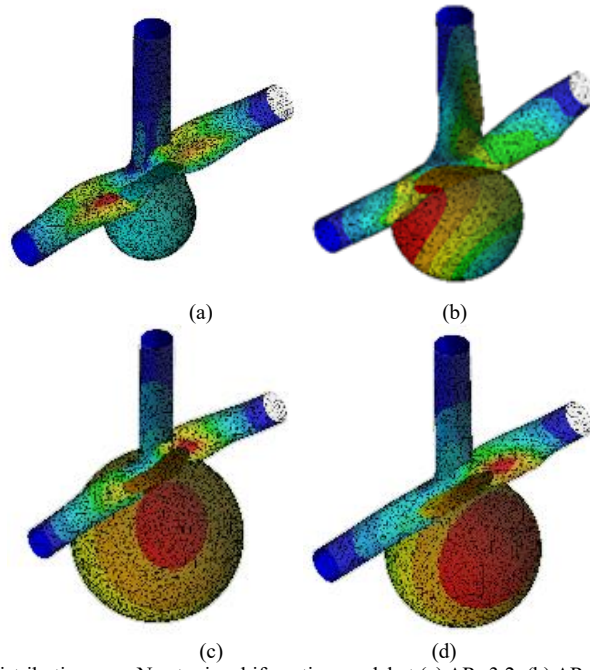
Figure 6. Von-Missess stress distribution, non-Newtonian, bifurcation model at (a) AR=3.2, (b) AR=4, (c) AR=4.8, and (d) AR= 5.6
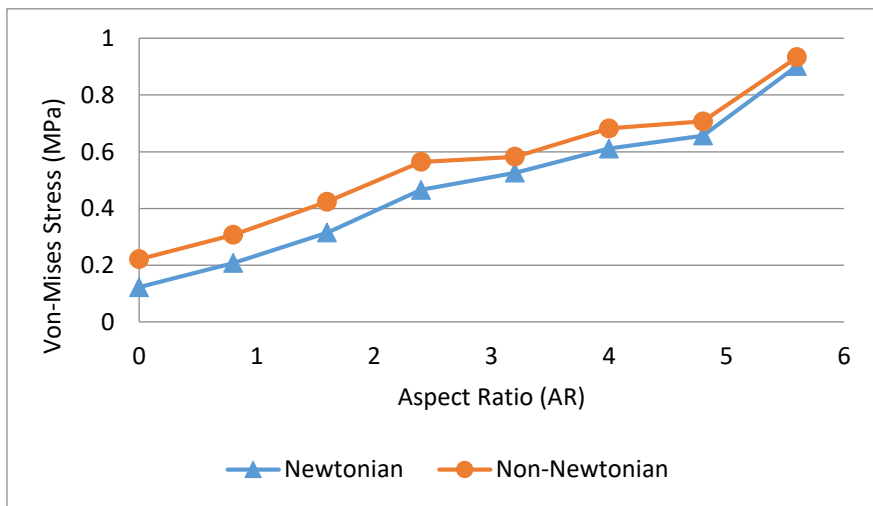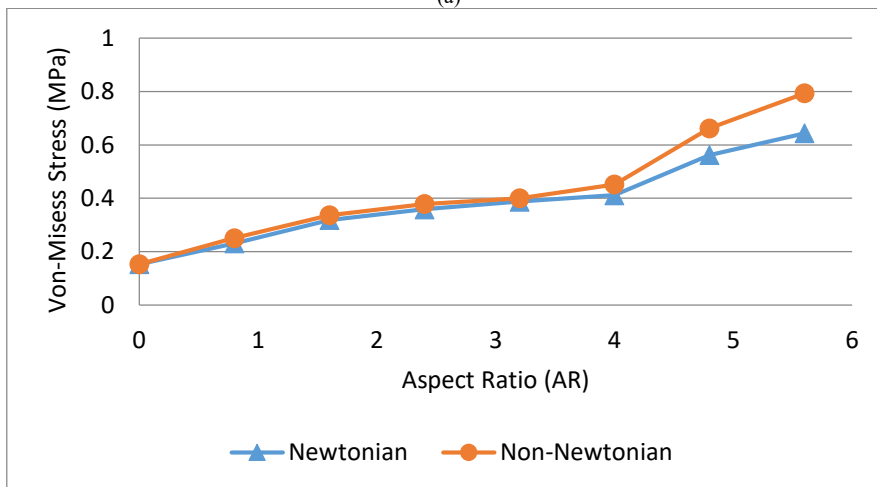
Figure 7. Von-Mises stress vs. aspect ratio for (a) non-bifurcation model, and (b) bifurcation model

Figure 7 demonstrates that $\sigma_{v.m}$ rises as the size of the aneurysm increases. Additionally, both bifurcation and non-bifurcation geometries exhibit an increase in the maximum $\sigma_{v.m}$ with increasing AR. This implies that as the aneurysm size expands, the maximum wall stress value also increases. This behavior resembles that of a thin spherical vessel, where the hoop stress in an aneurysm can be described by the relationship $\sigma = \frac{pd_a}{4t_{an}}$, taking into account the pressure (p), aneurysm diameter (d_a), and aneurysm thickness (t_{an}). Similarly, the longitudinal stress in the main artery can be described by the relationship $\sigma = \frac{pd_t}{4t_a}$, considering the pressure (p), diameter (d_t), and thickness (t_a), resembling the behavior of a thin cylindrical vessel.

In the context of blood flow, it is assumed that blood behaves as a Newtonian fluid when subjected to high shear stress rates (>100/s) in large arteries. However, in small artery sizes, blood is considered a non-Newtonian fluid. In Newtonian fluids, the shear stress is directly proportional to both the constant dynamic viscosity and the shear rate. On the other hand, non-Newtonian fluids exhibit a more complex relationship between viscosity and shear rate.

In Newtonian fluids, viscosity remains constant and serves as the proportionality factor between shear rate and shear stress. In contrast, the viscosity of non-Newtonian fluids depends on the shear rate but is independent of time and does not retain any kinematic history. This means that while a shear rate is being applied, the apparent viscosity of the non-Newtonian fluid may increase or decrease, but it will return to its original value once the fluid comes to rest.

In the case of blood, its apparent viscosity decreases as the shear rate increases, a phenomenon referred to as shear thinning viscosity, as also mentioned in Nader et al. [67] study.

The term "blood-thinning" primarily refers to the rheological properties of red blood cells. The flow of blood in the microcirculation heavily relies on the deformability of red blood cells. However, the deformation of these cells also impacts blood flow in the larger circulation, as reduced deformability leads to increased blood viscosity. According to Poiseuille's law, an increase in blood viscosity is expected to elevate vascular resistance. Moreover, higher blood viscosity can contribute to events resembling vasodilation and vascular occlusion, it is discussed also by Pinho et al. [68].

Considering that the thickness of the artery wall remains constant and the aneurysm walls are relatively thin, it is anticipated that the wall stress in the aneurysm region would be higher compared to the artery region. The enlargement of the aneurysm further applies pressure on the surrounding tissues and nerves. Based on Figure 7, we have established correlations to describe the relationship between $\sigma_{v.m}$ and the AR of both non-bifurcation and bifurcation models. These correlations can serve as indicators for identifying yielding at different aspect ratios.

For non-bifurcation model,

$$\sigma_{v.m} = \{0.11AR + 0.23 \quad Non-Newtonian\} \tag{11}$$

For bifurcation model

$$\sigma_{v.m} = \{0.09AR + 0.15 \quad Non-Newtonian\} \tag{12}$$

Figures 8 and 9 illustrate the aneurysm wall deformation and strain, which are additional factors requiring analysis.

It is observed that the deformation and strain remain largely unchanged with an increased AR up to AR≈ 1, exhibiting almost linear behavior within the range of $1 \leq AR \leq 5$. However, beyond that threshold, both deformation (Figure 8) and strain (Figure 9) exhibit a substantial increase as the AR increases. To establish the relationship between deformation/strain and AR, we employ curve fitting techniques to analyze the Figures presenting wall deformation and strain as functions of the AR. The resulting correlations are as follows:

For non-bifurcation model

$$\Delta L = \begin{cases} 0.9 - 2.65AR & 0 < AR < 1.0 \quad Non-Newtonian \\ 0.38AR + 0.39 & 5.6 \leq AR \geq 1.0 \; Non-Newtonian \end{cases} \tag{13}$$

For bifurcation model

$$\Delta L = \begin{cases} 0.9 - 4.96AR & 0 < AR < 1.0 \quad Non-Newtonian \\ 0.64AR - 0.47 & 5.6 \leq AR \geq 1.0 \quad Non-Newtonian \end{cases} \tag{14}$$

These established correlations provide valuable insights for estimating the yield starting point, which can assist in determining the necessity of surgical intervention. Additionally, the relationships between wall deformation, strain, and the aneurysm AR serve as useful indicators for estimating the time remaining before an aneurysm rupture may occur.
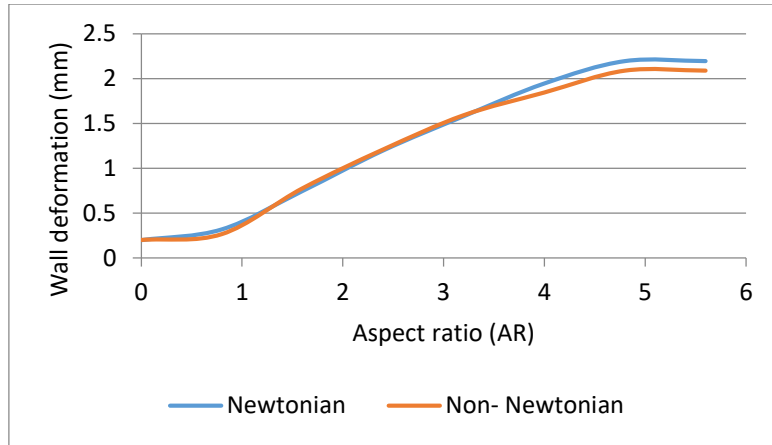
(a)
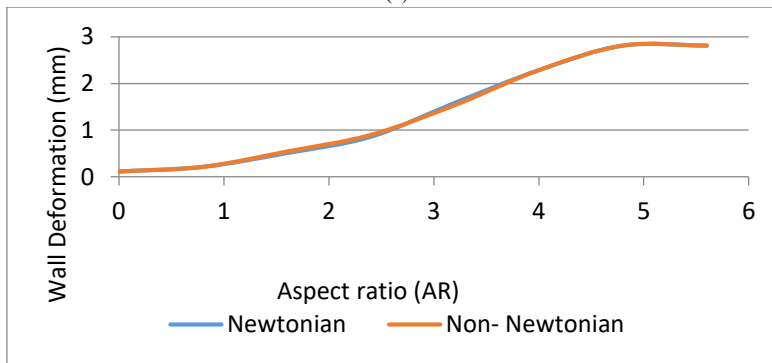
(b)

Figure 8. Wall deformation vs. aspect ratio for (a) non-bifurcation model and (b) bifurcation model
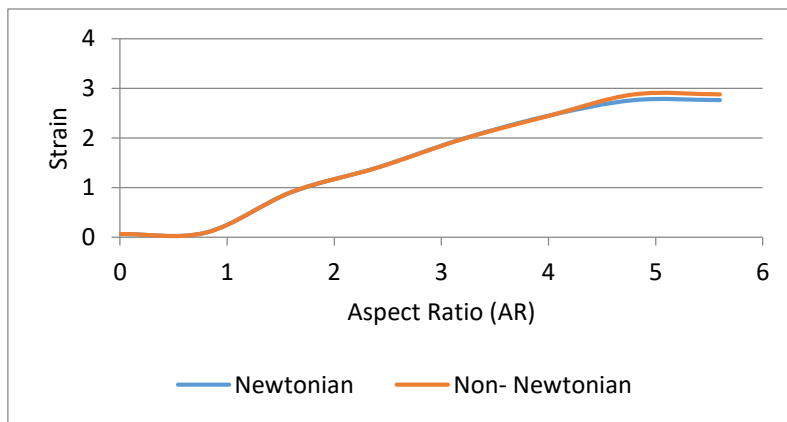
(a)
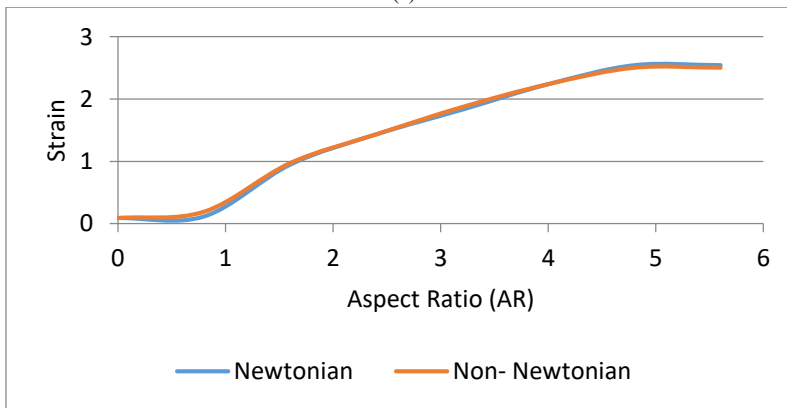
(b)

Figure 9. Strain vs. aspect ratio for (a) non-bifurcation model and (b) bifurcation model

To ensure the accuracy of our computational simulations and obtained results, we employed idealized models adapted from the patient-specific model by Sherif et al. [59] and Bazilevs et al. [46, 47]. We utilized boundary conditions from Sinnott et al. [63] and Netlyukh et al. [65]. The hemodynamic behavior generated by our numerical model was compared to results from other studies to validate our approach.

In terms of WSS values, our validation results, comparing them with Sun et al. [69], exhibited a maximum error of less than 9%, which is considered acceptable. A comparison of Von Mises stress values and the location of maximum stress in our research with Razaghi et al. [70] demonstrated relatively similar behavior, with an acceptable error of 6.7%.

Furthermore, when comparing the dynamic response of artery deformation and strain in our aneurysm simulation with Paz et al. [25] and Sun et al. [69], similar behavior was observed. These findings serve to validate both our computational methodology and the reliability of our hemodynamic simulations.

4. Conclusion

The FSI analysis in this study focused on CA models. The loads were computed numerically by constructing the fluid model using ANSYS Fluent, while the structural model was created using ANSYS Mechanical. The interaction between these two solutions was obtained using system coupling in the ANSYS Workbench.

Two idealized geometry models were used to show the effect of hemodynamic parameters on aneurysm formation, growth, and rupture. These parameters include blood velocity, viscosity, WSS, Von-Mises stress, wall deformation, and strain. Newtonian results were compared with those obtained using the non-Newtonian (Carreau) model for the blood viscosity modeling. It is observed that using the non-Newtonian model is more appropriate when dealing with low-velocity values and low WSS values zone, as is the case in an enlarging aneurysm.

Additionally, it was observed that the $\overline{WSS}$ reduced as the aneurysm AR increased. The same trend was observed for the maximum value of WSS. This reduction in WSS is attributed to the decrease in velocity associated with the enlargement of the aneurysm.

REFERENCES

[1] M. Sharzehee, S. S. Khalafvand, H. C. Han, "Fluid-structure interaction modeling of aneurysmal arteries under steady-state and pulsatile blood flow: a stability analysis", Computer Methods in Biomechanics and Biomedical Engineering, Vol. 21, No. 3, 2018, pp. 219-231. https://doi.org/10.1080/10255842.2018.1439478.

[2] Yu Y. Fluid-Structure Interaction Modeling in 3D Cerebral Arteries and Aneurysms. In: Wriggers, P., Lenarz, T. (eds) Biomedical Technology. Lecture Notes in Applied and Computational Mechanics, vol 84. Springer, Cham; 2018, pp. 123-146. https://doi.org/10.1007/978-3-319-59548-1_8.

[3] K. Valen-Sendstad, D. A. Steinman, "Mind the Gap: Impact of Computational Fluid Dynamics Solution Strategy on Prediction of Intracranial Aneurysm Hemodynamics and Rupture Status Indicators", American Journal of Neuroradiology, Vol. 35, No. 3, 2014, pp. 536-543. https://doi.org/10.3174/ajnr.A3793.

[4] M. Poueinak, S. Abdollahi, A. Alizadeh, M. Youshanlui, H. Zekri, M. Gerdroodbary, "Computational Study of Blood Hemodynamic in ICA Aneurysm with Coiling Embolism", International Journal of Modern Physics C, Vol. 34, No. 10, 2023, p. 2350138. https://doi.org/10.1142/S0129183123501383.

[5] Sabernaeemi, M. B. Gerdroodbary, S. Salavatidezfouli, P. Valipour, "Influence of Stent-Induced Vessel Deformation on Hemodynamic Feature of Bloodstream Inside ICA Aneurysms", Biomechanics and Modeling in Mechanobiology, Vol. 22, 2023, pp. 1193–1207. https://doi.org/10.1007/s10237-023-01710-9.

[6] S. Salavatidezfouli, A. Alizadeh, M. B. Gerdroodbary, A. Sabernaeemi, A. M. Abazari, A. Sheidani, "Investigation of the Stent Induced Deformation on Hemodynamic of Internal Carotid Aneurysms by Computational Fluid Dynamics", Scientific Reports, Vol. 13, 2023, p. 7155. https://doi.org/10.1038/s41598-023-34383-6.

[7] X. Y. Shen, M. B. Gerdroodbary, A. M. Abazari, R. Moradi, "Computational Study of Blood Flow Characteristics on Formation of the Aneurysm in the Internal Carotid Artery", The European Physical Journal Plus, Vol. 136, No. 5, 2021, p. 541. https://doi.org/10.1140/epjp/s13360-021-01545-2

[8] F. He, L. Hua, T. Guo, "Numerical Modeling in Arterial Hemodynamics Incorporating Fluid-Structure Interaction and Microcirculation", Theoretical Biology and Medical Modelling, Vol. 18, No. 1, 2021, pp. 1-10. https://doi.org/10.1186/s12976-021-00136-z.

[9] R. Savabi, M. Nabaei, S. Farajollahi, N. Fatouraee, "Fluid Structure Interaction Modeling of Aortic Arch and Carotid Bifurcation as the Location of Baroreceptors", International Journal of Mechanical Sciences, Vol. 165, 2020, p. 105222. https://doi.org/10.1016/j.ijmecsci.2019.105222.

[10] K. C. Cho, H. Yang, J. J. Kim, J. H. Oh, Y. B. Kim, "Prediction of Rupture Risk in Cerebral Aneurysms by Comparing Clinical Cases with Fluid–Structure Interaction Analyses", Scientific reports, Vol. 10, No. 1, 2020, p. 18237. https://doi.org/10.1038/s41598-020-75362-5.

[11] H. T. Sun, K. Y. Sze, A. Y. S. Tang, A. C. O. Tsang, A. C. H. Yu, K. W. Chow, "Effects of Aspect Ratio, Wall Thickness and Hypertension in the Patient-Specific Computational Modeling of Cerebral Aneurysms using Fluid-Structure Interaction Analysis", Engineering Applications of Computational Fluid Mechanics, Vol. 13, No. 1, 2019, pp. 229-244. https://doi.org/10.1080/19942060.2019.1572540.

[12] K. M. Saqr, "Computational Fluid Dynamics Simulations of Cerebral Aneurysm using Newtonian, Power-Law and Quasi-Mechanistic Blood Viscosity Models", Proceedings of the Institution of Mechanical Engineers, Part H: Journal of Engineering in Medicine, Vol. 234, No. 7, 2020, 711-719. https://doi.org/10.1177/0954411920917531.

[13] S. Gholampour, S. Mehrjoo, "Effect of Bifurcation in the Hemodynamic Changes and Rupture Risk of Small Intracranial Aneurysm", Neurosurgical Review, Vol. 44, No. 3, 2021, pp. 1703-1712. https://doi.org/10.1007/s10143-020-01367-3.

[14] J. G. Isaksen, Y. Bazilevs, T. Kvamsdal, Y. Zhang, J. H. Kaspersen, K. Waterloo, B. Romner, T. Ingebrigtsen, "Determination of Wall Tension in Cerebral Artery Aneurysms by Numerical Simulation", Stroke, Vol. 39, No. 12, 2008, pp. 3172-3178. https://doi.org/10.1161/STROKEAHA.107.503698.

[15] H. Jiang, Z. Lu, M. B. Gerdroodbary, A. Sabernaeemi, S. Salavatidezfouli, "The Influence of Sac Centreline on Saccular Aneurysm Rupture: Computational Study", Scientific Reports, Vol. 13, No. 1, 2023, p. 11288. https://doi.org/10.1038/s41598-023-38466-2.

[16] Sadeh, A. Kazemi, M. Bahramkhoo, M. B. Gerdroodbary, "Computational Analysis of the Blood Hemodynamic inside Internal Cerebral Aneurysm in the Existence of Endovascular Coiling", International Journal of Modern Physics C, Vol. 34, No. 5, 2023, p. 2350059. https://doi.org/10.1142/S0129183123500596.

[17] S. Hariri, M. M. Poueinak, A. Hassanvand, M. B. Gerdroodbary, M. Faraji, "Effects of Blood Hematocrit on Performance of Endovascular Coiling for Treatment of Middle Cerebral Artery (MCA) Aneurysms: Computational Study", Interdisciplinary Neurosurgery, Vol. 32, 2023, p. 101729. https://doi.org/10.1016/j.inat.2023.101729.

[18] Kleinstreuer, Z. Li, M. A. Farber, "Fluid-Structure Interaction Analyses of Stented Abdominal Aortic Aneurysms", Annual Review of Biomedical Engineering, Vol. 9, No. 1, 2007, pp. 169-204. https://doi.org/10.1146/annurev.bioeng.9.060906.151853.

[19] M. Xenos, S. H. Rambhia, Y. Alemu, S. Einav, N. Labropoulos, A. Tassiopoulos, J. J. Ricotta, D. Bluestein, "Patient-Based Abdominal Aortic Aneurysm Rupture Risk Prediction with Fluid Structure Interaction Modeling", Annals of Biomedical Engineering, Vol. 38, No. 11, 2010, pp. 3323-3337. https://doi.org/10.1007/s10439-010-0094-3.

[20] M. Scotti, A. D. Shkolnik, S. C. Muluk, E. A. Finol, "Fluid-Structure Interaction in Abdominal Aortic Aneurysms: Effects of Asymmetry and Wall Thickness", BioMedical Engineering OnLine, Vol. 4, No. 1, 2005, pp. 1-22. https://doi.org/10.1186/1475-925x-4-64.

[21] A. Rostam-Alilou, H. R. Jarrah, A. Zolfagharian, M. Bodaghi, "Fluid–Structure Interaction (FSI) Simulation for Studying the Impact of Atherosclerosis on Hemodynamics, Arterial Tissue Remodeling, and Initiation Risk of Intracranial Aneurysms," Biomechanics and Modeling in Mechanobiology, Vol. 21, No. 5, 2022, pp. 1393-1406. https://doi.org/10.1007/s10237-022-01597-y.

[22] S. R Shine, S. Saha, E. Harshavardhan, B. J. Sudhir, "Fluid–Structure Interaction Model for Assessing Aneurysm Initiation at the Circle of Willis", Journal of Engineering and Science in Medical Diagnostics and Therapy, Vol. 5, No. 3, 2022, p. 031101. https://doi.org/10.1115/1.4053843.

[23] R. Abdollahi, B. Vahidi, P. Shojaee, M. Karimi, "A Comparative Study between CFD and FSI Hemodynamic Parameters in a Patient-Specific Giant Saccular Cerebral Aneurysm", AUT Journal of Modeling and Simulation, Vol. 53, No. 1, 2021, pp. 23-38. https://doi.org/10.22060/miscj.2020.18742.5222.

[24] T. AlMomani, S. Bani Hani, O. Smadi, S. Alzghoul, L. Kiswani, M. Assarsour, "The Influence of Internal Carotid Artery off-plane Angle on the Hemodynamics of Blood Flow in the Carotid Artery", Jordan Journal of Mechanical and Industrial Engineering, Vol. 13, No. 3, 2019, pp.141-148.

[25] Paz, E. Suarez, A. Cabarcos, S. I. S. Pinto, "FSI Modeling on the Effect of Artery-Aneurysm Thickness and Coil Embolization in Patient Cases", Computer Methods and Programs in Biomedicine, Vol. 206, 2021, p. 106148. https://doi.org/10.1016/j.cmpb.2021.106148.

[26] K. Khe, A. A. Cherevko, A. P. Chupakhin, M. S. Bobkova, A. L. Krivoshapkin, K. Y. Orlov, "Haemodynamics of Giant Cerebral Aneurysm: A Comparison between the Rigid-Wall, One-Way and Two-Way FSI Models", Journal of Physics: Conference Series, Vol. 722, 2016, p. 012042. https://doi.org/10.1088/1742-6596/722/1/012042.

[27] M. Fattahi, S. A. Abdollahi, A. H. Alibak, S. Hosseini, P. L. Dang, "Influence of Parent Vessel Feature on the Risk of Internal Carotid Artery Aneurysm Rupture via Computational Method", Scientific Reports, Vol. 13, No. 1, 2023, p. 20544. https://doi.org/10.1038/s41598-023-47927-7.

[28] M. Fattahi, S. A. Abdollahi, A. H. Alibak, S. Hosseini, P. L. Dang, "Usage of Computational Method for Hemodynamic Analysis of Intracranial Aneurysm Rupture Risk in Different Geometrical Aspects", Scientific Reports, Vol. 13, No. 1, 2023, P. 20749. https://doi.org/10.1038/s41598-023-48246-7.

[29] K. Hajirayat, S. Gholampour, I. Sharifi, D. Bizari, "Biomechanical Simulation to Compare the Blood Hemodynamics and Cerebral Aneurysm Rupture Risk in Patients with Different Aneurysm Necks", Journal of Applied Mechanics and Technical Physics, Vol. 58, No. 6, 2017, pp. 968-974. https://doi.org/10.1134/s0021894417060025.

[30] Sheidani, M. B. Gerdroodbary, A. Poozesh, A. Sabernaeemi, S. Salavatidezfouli, A. Hajisharifi, "Influence of the Coiling Porosity on the Risk Reduction of the Cerebral Aneurysm Rupture: Computational Study," Scientific Reports, Vol. 12, No. 1, 2022, p. 19082. https://doi.org/10.1038/s41598-022-23745-1.

[31] F. P. P. Tan, R. Torii, A. Borghi, R. H. Mohiaddin, N. B. Wood, X. Y. Xu, "Fluid-Structure Interaction Analysis of Wall Stress and Flow Patterns in a Thoracic Aortic Aneurysm", International Journal of Applied Mechanics, Vol. 1, No. 1, 2009, pp. 179-199. https://doi.org/10.1142/S1758825109000095.

[32] J. Lantz, J. Renner, M. Karlsson, "Wall Shear Stress in a Subject Specific Human Aorta—Influence of Fluid-Structure Interaction", International Journal of Applied Mechanics, Vol. 3, No. 4, 2011, pp. 759–778. https://doi.org/10.1142/s1758825111001226.

[33] M. Alimohammadi, J. M. Sherwood, M. Karimpour, O. Agu, S. Balabani, V. Díaz-Zuccarini, "Aortic Dissection Simulation Models for Clinical Support: Fluid-Structure Interaction vs. Rigid Wall Models", BioMedical Engineering OnLine, Vol. 14, No. 1, 2015, pp. 1-16. https://doi.org/10.1186/s12938-015-0032-6.

[34] R. Torii, N. B. Wood, N. Hadjiloizou, A. W. Dowsey, A. R. Wright, A. D. Hughes, Justin Davies et al., "Fluid–Structure Interaction Analysis of a Patient-Specific Right Coronary Artery with Physiological Velocity and Pressure Waveforms", Communications in numerical methods in engineering, Vol. 25, No. 5, 2009, pp. 565-580. https://doi.org/10.1002/cnm.1231.

[35] X. Bai-Nan, W. Fu-Yu, L. Lei, Z. Xiao-Jun, J. Hai-Yue, "Hemodynamics Model of Fluid–Solid Interaction in Internal Carotid Artery Aneurysms", Neurosurgical review, Vol. 34, No. 1, 2011, pp. 39-47. https://doi.org/10.1007/s10143-010-0282-5.

[36] K. Luo, W. Jiang, Y. Chen, X. Tian, Z. Zhou, D. Yuan, "Fluid–Solid Interaction Analysis on Iliac Bifurcation Artery: A Numerical Study", International Journal of Computational Methods, Vol. 16, No. 7, 2019, pp. 1850112–1850112. https://doi.org/10.1142/s0219876218501128.

[37] M. Jahangiri, M. Saghafian, M. R. Sadeghi, "Numerical Simulation of Non-Newtonian Models Effect on Hemodynamic Factors of Pulsatile Blood Flow in Elastic Stenosed Artery", Journal of Mechanical Science and Technology, Vol. 31, No. 2, 2017, pp. 1003-1013. https://doi.org/10.1007/s12206-017-0153-x.

[38] S. Frecentese, L. P. Argani, A. B. Movchan, N. V. Movchan, G. Carta, M. L. Wall, "Waves and Fluid–Solid Interaction in Stented Blood Vessels", Proceedings of The Royal Society A: Mathematical, Physical and Engineering Sciences, Vol. 474, No. 2209, 2018, pp. 20170670-20170670. https://doi.org/10.1098/rspa.2017.0670.

[39] R. Torii, M. Oshima, T. Kobayashi, K. Takagi, T. E. Tezduyar, "Fluid–Structure Interaction Modeling of Aneurysmal Conditions with High and Normal Blood Pressures", Computational Mechanics, Vol. 38, No. 4-5, 2006, pp. 482-490. https://doi.org/10.1007/s00466-006-0065-6.

[40] S. Ahmed, I. D. Sutalo, H. Kavnoudias, A. Madan, "Fluid Structure Interaction Modelling of a Patient Specific Cerebral Aneurysm: Effect of Hypertension and Modulus of Elasticity". 16th Australasian Fluid Mechanics Conference, Gold Coast, Australia, 2007.

[41] Y. Feng, S. Wada, T. Ishikawa, K. I. Tsubota, T. Yamaguchi, "A Rule-Based Computational Study on the Early Progression of Intracranial Aneurysms using Fluid-Structure Interaction: Comparison between Straight Model and Curved Model", Journal of Biomechanical Science and Engineering, Vol. 3, No. 2, 2008, pp. 124-137. https://doi.org/10.1299/jbse.3.124.

[42] R. Torii, M. Oshima, T. Kobayashi, K. Takagi, T. E. Tezduyar, "Fluid–Structure Interaction Modeling of a Patient-Specific Cerebral Aneurysm: Influence of Structural Modeling", Computational Mechanics, Vol. 43, No. 1, 2008, pp. 151-159. https://doi.org/10.1007/s00466-008-0325-8.

[43] R. Torii, M. Oshima, T. Kobayashi, K. Takagi, T. E. Tezduyar, "Influence of Wall Thickness on Fluid-Structure Interaction Computations of Cerebral Aneurysms", Vol. 26, No. 3-4, 2010, pp. 336-347. https://doi.org/10.1002/cnm.1289.

[44] Á. Valencia, D. Ledermann, R. Rivera, E. Bravo, M. Gálvez, "Blood Flow Dynamics and Fluid-Structure Interaction in Patient-Specific Bifurcating Cerebral Aneurysms", International Journal for Numerical Methods in Fluids, Vol. 58, No. 10, 2008, pp. 1081-1100. https://doi.org/10.1002/fld.1786.

[45] K. Takizawa et al., "Patient-Specific Arterial Fluid–Structure Interaction Modeling of Cerebral Aneurysms", International Journal for Numerical Methods in Fluids, Vol. 65, No. 1-3, 2010, pp. 308-323. https://doi.org/10.1002/fld.2360.

[46] Y. Bazilevs et al., "A Fully-Coupled Fluid-Structure Interaction Simulation of Cerebral Aneurysms", Computational Mechanics, Vol. 46, No. 1, 2009, pp. 3-16. https://doi.org/10.1007/s00466-009-0421-4.

[47] Y. Bazilevs et al., "Computational Vascular Fluid–Structure Interaction: Methodology and Application to Cerebral Aneurysms", Biomechanics and Modeling in Mechanobiology, Vol. 9, No. 4, 2010, pp. 481-498. https://doi.org/10.1007/s10237-010-0189-7.

[48] K. Takizawa, T. Brummer, T. E. Tezduyar, P. R. Chen, "A Comparative Study Based on Patient-Specific Fluid-Structure Interaction Modeling of Cerebral Aneurysms", Journal of Applied Mechanics, Vol. 79, No. 1, 2012, p. 010908. https://doi.org/10.1115/1.4005071.

[49] J. Lee, Y. Zhang, H. Takao, Y. Murayama, Y. Qian, "A Fluid–Structure Interaction Study using Patient-Specific Ruptured and Unruptured Aneurysm: The Effect of Aneurysm Morphology, Hypertension and Elasticity", Journal of Biomechanics, Vol. 46, No. 14, 2013, pp. 2402-2410. https://doi.org/10.1016/j.jbiomech.2013.07.016.

[50] T. Qiu, G. Jin, W. Bao, H. Lu, "Intercorrelations of Morphology with Hemodynamics in Intracranial Aneurysms in Computational Fluid Dynamics", Neurosciences, Vol. 22, No. 3, 2017, pp. 205-212. https://doi.org/10.17712/nsj.2017.3.20160452.

[51] Shamloo, M. A. Nejad, M. Saeedi, "Fluid–Structure Interaction Simulation of a Cerebral Aneurysm: Effects of Endovascular Coiling Treatment and Aneurysm Wall Thickening", Journal of the Mechanical Behavior of Biomedical Materials, Vol. 74, 2017, pp. 72-83. https://doi.org/10.1016/j.jmbbm.2017.05.020.

[52] Á. Valencia, F. Torres, "Effects of Hypertension and Pressure Gradient in a Human Cerebral Aneurysm using Fluid Structure Interaction Simulations", Journal of Mechanics in Medicine and Biology, Vol. 17, No. 1, 2017,

pp. 1750018-1750018. https://doi.org/10.1142/s021951941750018x.

[53] Avolio et al., "Cerebral Haemodynamics: Effects of Systemic Arterial Pulsatile Function and Hypertension", Current Hypertension Reports, Vol. 20, No. 3, 2018, pp. 1-11. https://doi.org/10.1007/s11906-018-0822-x.

[54] S. Shawish, D. Bani Mostafa, R. Alwaked, M. S. Nasif, "CFD Simulation of Energy Transfer within a Membrane Heat Exchanger under Turbulent Flow", Jordan Journal of Mechanical and Industrial Engineering, Vol. 17, No. 2, 2023, pp. 139-154. https://doi.org/10.59038/jjmie/170201.

[55] M. Saraireh, "Computational Fluid DynamicsSimulation of Plate Fin and Circular Pin Fin Heat Sink", Jordan Journal of Mechanical and Industrial Engineering, Vol. 10, No. 2, 2016, pp. 99-104.

[56] Alshare, W. Al-Kouz, S. Kiwan, A. Al-khalidi, M. Hader, "Computational Modeling of Gaseous Flow and Heat Transfer in a Wavy Microchannel", Jordan Journal of Mechanical and Industrial Engineering, Vol. 10, No. 1, 2016, pp.75-83.

[57] R. Ali, A. Singh, "Numerical Study of Fluid Dynamics and Heat Transfer Characteristics for the Flow Past a Heated Square Cylinder", Jordan Journal of Mechanical and Industrial Engineering, Vol. 15, No. 4, 2021, pp.357-376.

[58] T. Ishibashi et al., "Unruptured Intracranial Aneurysms: Incidence of Rupture and Risk Factors", Stroke, Vol. 40, No. 1, 2009, pp. 313-316. https://doi.org/10.1161/strokeaha.108.521674.

[59] Sherif et al., "Evaluation of cerebral aneurysm wall thickness in experimental aneurysms: Comparison of 3T-MR imaging with direct microscopic measurements", Acta Neurochirurgica, Vol. 156, No. 1, 2014, pp. 27-34. https://doi.org/10.1007/s00701-013-1919-2.

[60] H. J. Steiger, R. Aaslid, S. Keller, H. J. Reulen, "Strength, Elasticity and Viscoelastic Properties of Cerebral Aneurysms", Heart and Vessels, Vol. 5, No. 1, 1989, pp. 41-46. https://doi.org/10.1007/bf02058357.

[61] T. Sochi, "Non-Newtonian Rheology in Blood Circulation", arXiv preprint arXiv:1306.2067. 2013.

[62] R. G. Gosling, M. M. Budge, "Terminology for Describing the Elastic Behavior of Arteries", Hypertension, Vol. 41, No. 6, 2003, pp. 1180-1182. https://doi.org/10.1161/01.hyp.0000072271.36866.2a.

[63] M. Sinnott, P. W. Cleary, M. Prakash, "An Investigation of Pulsatile Blood Flow in a Bifurcation Artery using a Grid-Free Method". Proc. Fifth International Conference on CFD in the Process Industries, pp. 1-6. 2006.

[64] P. Waldenberger, A. Chemelli, and A. Mallouhi, "Intra-Arterial Haemodynamic Changes during Cerebral Three-Dimensional Rotational Angiography", European Radiology, Vol. 19, No. 2, 2009, pp. 503-508. https://doi.org/10.1007/s00330-008-1161-0.

[65] M. Netlyukh, V. M. Shevaga, L. M. Yakovenko, A. V. Payenok, V. M. Salo, O. J. Kobyletskiy, "Invasive Intracranial Arterial Pressure Monitoring During Endovascular Cerebral Aneurysms Embolization for Cerebral Perfusion Evaluation". In: Fandino, J., Marbacher, S., Fathi, AR., Muroi, C., Keller, E. (eds) Neurovascular Events After Subarachnoid Hemorrhage. Acta Neurochirurgica Supplement, Vol 120, 2015, pp. 177-181. Springer, Cham. https://doi.org/10.1007/978-3-319-04981-6_30.

[66] Valencia, H. Morales, R. Rivera, E. Bravo, M. Galvez, "Blood Flow Dynamics in Patient-Specific Cerebral Aneurysm Models: The Relationship Between Wall Shear Stress and Aneurysm Area Index", Medical Engineering and Physics, Vol. 30, No. 3, 2008, pp. 329-340. https://doi.org/10.1016/j.medengphy.2007.04.011.

[67] Nader et al., "Blood Rheology: Key Parameters, Impact on Blood Flow, Role in Sickle Cell Disease and Effects of

Exercise", Frontiers in Physiology, Vol. 10, 2019, p. 1329. https://doi.org/10.3389/fphys.2019.01329.

[68] Pinho, V. Carvalho, I. M. Gonçalves, S. Teixeira, R. Lima, "Visualization and Measurements of Blood Cells Flowing in Microfluidic Systems and Blood Rheology: A Personalized Medicine Perspective", Journal of Personalized Medicine, Vol. 10, No. 4, 2020, p. 249. https://doi.org/10.3390/jpm10040249.

[69] H. T. Sun, K. Y. Sze, K. W. Chow, A. C. On Tsang, "A comparative Study on Computational Fluid Dynamic, Fluid-Structure Interaction and Static Structural Analyses of Cerebral Aneurysm", Engineering Applications of Computational Fluid Mechanics, Vol. 16, No. 1, 2022, pp. 262-278. https://doi.org/10.1080/19942060.2021.2013322.

[70] R. Razaghi, H. Biglari, A. Karimi, "Risk of Rupture of the Cerebral Aneurysm in Relation to Traumatic Brain Injury using a Patient-Specific Fluid-Structure Interaction Model", Computer Methods and Programs in Biomedicine, Vol. 176, 2019, pp. 9-16. https://doi.org/10.1016/j.cmpb.2019.04.015.